From ZnO Nanorods to Nanoplates: Chemical Bath Deposition Growth and Surface-Related Emissions

Bingqiang Cao*,† and Weiping Cai

Key Lab of Materials Physics and Anhui Kay Lab of Nanomaterials and Nanotechnology, Institute of Solid State Physics, Chinese Academy of Sciences, Hefei, 230031, Anhui, China

Received: August 28, 2007; In Final Form: October 2, 2007

In this paper, a low-temperature controllable chemical bath deposition method was demonstrated to prepare one-dimensional ZnO nanorods and two-dimensional nanoplates, and their surface-related emissions were studied by temperature-dependent cathodoluminescence spectra. By changing the precursor concentration, the ZnO morphology evolves from nanorods to nanoplates. ZnO nanorods grow fast along the *c*-axis direction due to the high surface energy of the polar (0001) plane when the concentration of OH^- ions is low in the precursor solution. When the OH^- concentration is increased, more OH^- ions preferably adsorb on the (0001) plane of ZnO, and the growth of the ZnO nanocrystallite along the *c* axis is partially suppressed. However, they can still grow sideways along $<2\bar{1}\bar{1}0>$ directions. Therefore, with the OH^- concentration increased, the average aspect ratio (high/width) of ZnO nanorods is decreased. Finally, two-dimensional ZnO nanoplates are formed. Low-temperature cathodoluminescence spectra of such ZnO nanostructures exhibit donor-bound exciton emission and surface-state-related exciton emission caused by surface impurities. With increasing temperature, the bound exciton emission decreases gradually due to the ionization of donors and finally vanishes when the temperature is above 130 K. The near-band-gap ultraviolet emission at room temperature is dominated by surface-related exciton emission.

1. Introduction

Zinc oxide (ZnO), a II−VI compound oxide semiconductor with a direct band gap of 3.37 eV and a high exciton binding energy of 60meV at room temperature, is an important kind of technological semiconductor due to its distinguished optical, electrical, and piezoelectrical properties, which can be widely used in optoelectronic and photovoltaic devices.[1,2] It manifests its applications especially when approaching the nanoscale size, for example, in the form of one-dimensional nanowires/nanorods/nanotubes[3] or two-dimensional nanoplates/nanosheets,[4−13] which have been widely accepted as the building blocks for nanodevices. In view of this point, controlled growth of nanostructures in terms of size, shape, and orientation is a prerequisite, and a large amount of intensive research has been conducted to prepare desired ZnO architectures. Until now, the thermal vapor transport and condensation method based on the vapor−liquid−solid (VSL) mechanism has been the most widely adapted strategy for the preparation of ZnO nanostructures. A variety of one-dimensional nanostructures like nanowires, nanobelts, nanorings, and other hierarchical nanostructures have been obtained through this strategy and used to construct functional devices.[14] However, due to their structural polarity, the preparation of two-dimensional ZnO nanostructures is still challenging, and the few reported ZnO nanosheets prepared by the vapor-phase method are of low optical quality.[5,6]

In comparison with vapor-phase methods, solution-phase methods are appealing for their cheap experimental setups, large productivity, and good potential for scale-up. Chemical bath deposition (CBD) is one of the useful solution methods for the preparation of compound semiconductors from aqueous solution, with advantages such as low processing temperature, allowing growth upon a variety of substrates, and easy adaptation to large area processing at low fabrication cost.[15] M. Izaki[16] has prepared highly (0001)-oriented ZnO films by UV light-assisted CBD from an aqueous solution containing hydrated zinc nitrate and dimethylamineborane (DMAB). A recent report has shown that the CBD method can be used to synthesize ZnO films and nanorod arrays on different substrates.[17] Li et al.[10] have prepared hexagonal ZnO nanoplates and nanorings by an organic template-assisted CBD method. However, for these solution methods, it is also difficult to control the growth of ZnO nanostructures with different morphologies.

Moreover, for the utilization of such ZnO nanostructures to construct optoelectronic devices, it is essential to fully understand their optical properties. Although a number of theoretical and experimental studies on the optical properties of ZnO quantum dots,[18,19] nanowires,[20,21] films,[22,23] as well as bulk crystals[24] have been reported, some properties of luminescence in ZnO are still not very clear now. One poorly understood issue is the exact mechanism of the near-band-gap (NBG) ultraviolet (UV) emission at room temperature. While it is well accepted that the low-temperature (∼10 K) emission of ZnO is dominated by the donor-bound exciton (D^0, X) and/or free exciton (FX) emissions,[25] there is no agreement about the mechanism of the emission at higher temperatures. Different studies have arrived at different conclusions that the room-temperature UV emission has been attributed to FX,[26] optical phonon replicas of FX,[27,28] (D^0, X),[29] bands of donor states,[30] acceptor-bound excitons (A^0, X),[31] and surface-related emissions.[32] As we know, the optical properties of semiconductors are mainly determined by the crystal quality and impurities, which are all closely related with

* To whom correspondence should be addressed. E-mail: Bingqiang.cao@physik.uni-leipzig.de.
† Present Address: Fakultät für Physik und Geowissenschaften, Universität Leipzig, Linnéstrasse 5, 04103 Leipzig, Germany

10.1021/jp076870l CCC: $40.75
Published on Web 12/29/2007

the preparation methods. Therefore, a study the optical properties of the ZnO nanostructures prepared by different methods is needed, especially the carrier recombination process at room temperature, which is the key to the use of the optical properties of such ZnO nanostructures and subsequent optoelectronic device development.

In this paper, we report a CBD method to prepare different ZnO nanostructures, evolving from one-dimensional nanorods to two-dimensional nanoplates, in a controllable way by changing the concentrations of precursors. A precursor concentration-induced growth mechanism is also proposed. Detailed temperature-dependent cathodoluminescence study of these ZnO nanostructures shows that the NBG UV emission at room temperature is mainly composed of surface-related exciton (SX) emissions probably caused by impurities on the surfaces.

2. Experimental Section

In a typical series of experiments, the precursor solution was composed of hydrated zinc nitrate ($Zn(NO_3)_2 \cdot 6H_2O$) with concentrations from 0.025 to 0.1 M and dimethylamineborane [DMAB, $(CH_3)_2NHBH_3$] of 0.05 M. All of the solutions were prepared with reagent-grade chemicals. Silicon substrate was cleaned with acetone in an ultrasonic bath and etched by piranha solution (2:1 mixture of concentrated H_2SO_4/30%H_2O_2) at room temperature for 30 min. Then, the silicon slice was dipped into an glass container that was filled with the nutrient solution mentioned above. Then, the covered reaction container was put into an oven that was maintained at 70 °C for around 3 h. Finally, the products on the silicon substrates were taken out and washed with deionized water. The as-prepared samples were then dried at 70 °C in air for further characterizations.

Field emission scanning electron microscopy (FESEM) (FEI, Sirion 200) and transmission electron microscopy (TEM) (H-800 and JEOL-2010) were used to examine the morphologies and microstructures of the samples. Phase identification of the sample was done with a Philips X'Pert powder X-ray diffractometer equipped with Cu Kα line ($\lambda = 0.15419$ nm) radiation. An energy dispersive X-ray spectrum (EDX, Inca, Oxford) was used to test the purity of the as-prepared samples. Temperature-dependent cathodoluminescence (CL) spectra were obtained in a scanning electron microscope of CamScan CS44 with 10 keV electron energy and a beam current of 150 pA. The wavelength respective energy scale of the CL spectra was calibrated prior to each set of measurements using a neon lamp. More technical detailed parameters of the CL system can be found in ref 33.

3. Results and Discussion

3.1. Structural Characterization. Figure 1a shows the powder X-ray diffraction (XRD) pattern of the as-synthesized products, where all diffraction peaks can be attributed to the wurtzite hexagonal ZnO (JCPDS 36−1451) with the measured lattice constants of a and c of 3.25 and 5.21 Å ($c/a = 1.60$), respectively. The XRD pattern indicates that the samples obtained via the CBD method only consist of a pure phase of ZnO. A typical EDX spectrum of Figure 1b shows that only O and Zn elements are detected, besides the silicon signal from the silicon substrate. All of the ZnO samples acquired in the experiments show the similar XRD and EDX characters as those displayed here. This proves that the as-prepared samples are all of pure ZnO phase.

The morphologies of the as-synthesized ZnO samples were characterized with SEM. Typical SEM images shown in Figure 2 were measured on the samples prepared from precursors consisting of $Zn(NO_3)_2$ with concentrations from 0.025 to 0.1 M and DMAB with fixed concentration of 0.05 M. When the $Zn(NO_3)_2$ concentrations are lower than 0.05 M, the general morphologies of the prepared ZnO samples shown in Figure 2a and b are nanorods with typical lengths of several micrometers and diameters of hundreds of nanometers. When the concentration of $Zn(NO_3)_2$ is increased to 0.075 M, mixtures of nanorods and plate-shaped (nanoplate) ZnO nanostructures are observed, as shown in Figure 2c. In comparison with the nanorods shown in Figure 1a and b, the aspect ratio (height to width) of the nanorod in Figure 3c is obviously smaller. As the concentration of $Zn(NO_3)_2$ is further increased, much purer ZnO nanoplates are prepared, as shown in Figure 2d. The ZnO nanoplates are typically hundreds of nanometers in thickness and several micrometers in dimension. Moreover, many nanoplates have regular edges with an angle of 120°, which corresponds to the angles between the {01−10} planes of the wurtzite ZnO crystal structure.

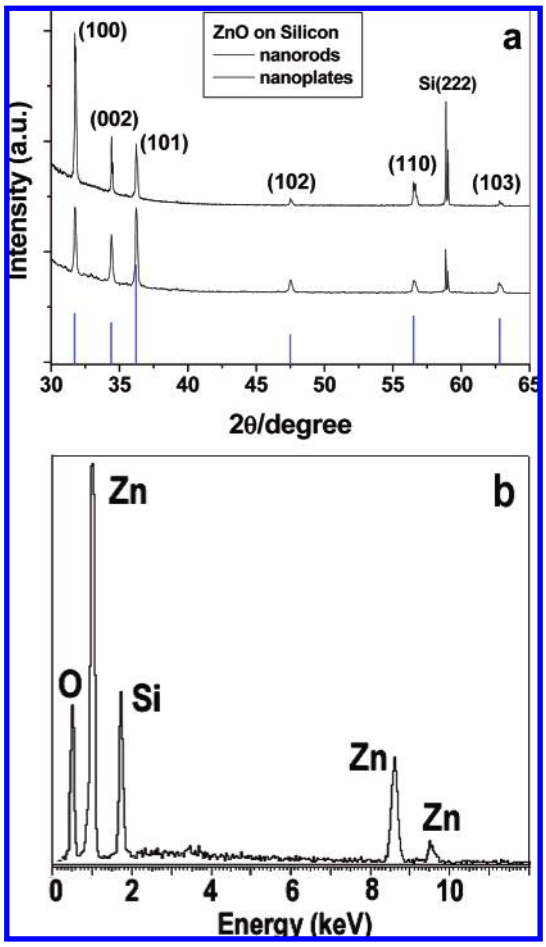

Figure 1. XRD (a) and EDX (b) spectra of the as-prepared samples on silicon substrates. Vertical lines in (a) are the responding XRD peaks of wurtzite ZnO powders from JCPDS (36−1451).

TEM was also applied to study the microstructure of the nanorods and nanoplates. A representative TEM image of ZnO nanorods is shown in Figure 3a. Its high-resolution TEM image shown in Figure 3b indicates that the ZnO nanorod is of single-crystal structure. It also clearly shows that the (0001) crystal planes are perpendicular to the axis of the nanorod, indicating that <0001> is the preferred growth direction of ZnO nanorods. The inset of Figure 3b is the corresponding selected area electron diffraction (SAED) pattern, which further proves the single-crystal nature of the nanorods and their <0001> growth direction. Figure 3c is the TEM and SAED image of ZnO nanoplates. Many nanoplates are rather regular hexagons, and

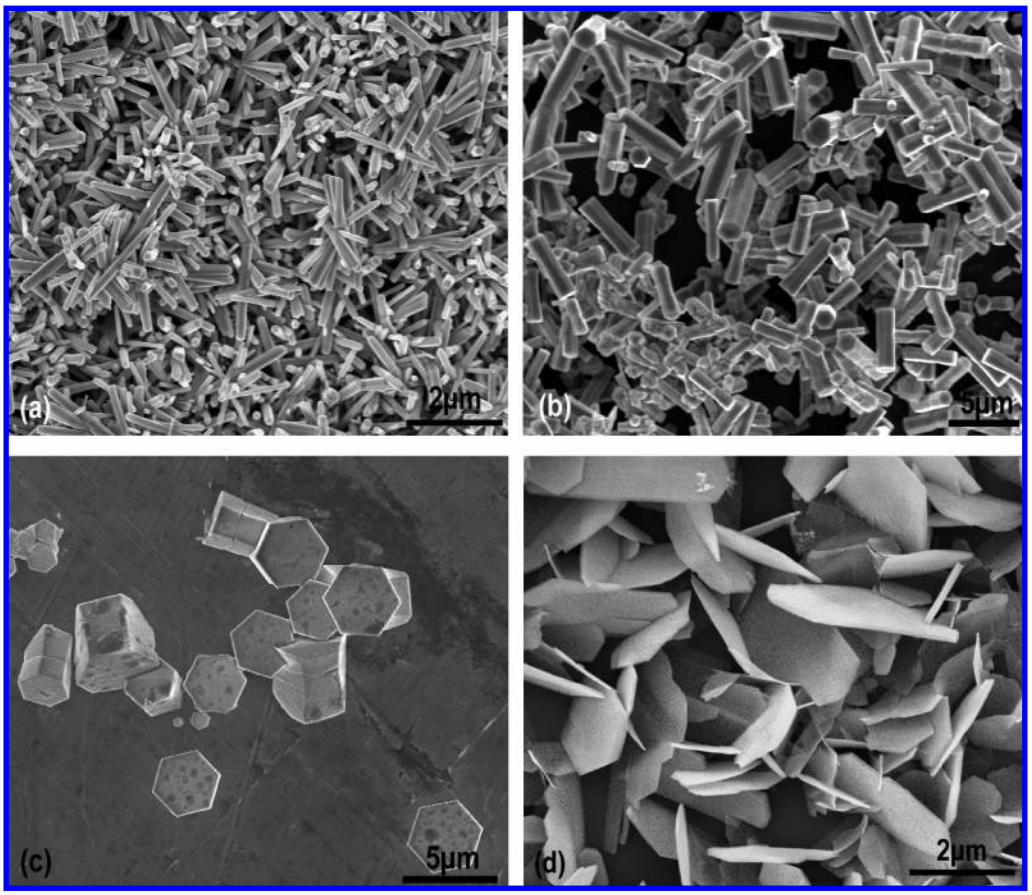

Figure 2. SEM images of the ZnO samples obtained from the precursor solutions composed of $Zn(NO_3)_2$ with different concentrations of (a) 0.025 M, (b) 0.05 M, (c) 0.75 M, (d) 0.1 M and DMAB of 0.05 M.

the contrast on a whole sheet is homogeneous. The inset SAED pattern can be indexed as a hexagonal ZnO along the [0001] axis and also proves the single-crystal structure of the nanoplate. A more detailed HRTEM study has proved that the top and bottom surfaces of the nanoplates are {0001} planes and the side facets correspond to the $\{01\bar{1}0\}$ planes.[12] Therefore, the crystal growth rate of such a ZnO nanoplate along $<2\bar{1}\bar{1}0>$ is faster than that of the <0001> direction.

3.2. Growth Mechanism. Now let us give a discussion on the growth mechanism of the ZnO nanorods and nanoplates prepared by the CBD method. The general chemical reaction mechanism in the precursor solution can be speculated to be as follows[34]

$$(CH_3)_2NHBH_3 + H_2O \rightarrow BO_2^- + (CH_3)_2NH + 7H^+ + 6e^- \quad (1)$$

$$Zn(NO_3)_2 \rightarrow Zn^{2+} + 2NO_3^- \quad (2)$$

$$NO_3^- + H_2O + 2e^- \rightarrow NO_2^- + 2OH^- \quad (3)$$

$$Zn^{2+} + 2OH^- + 2H_2O \rightarrow Zn(OH)_4^{2-} + 2H^+ \quad (4)$$

$$Zn(OH)_4^{2-} + 2H^+ \rightarrow ZnO_{cluster} + 3H_2O \quad (5)$$

In the chemical solution, the DMAB is first hydrolyzed, and free electrons are released at the same time (eq 1). Therefore, the NO_3^- ions can acquire electrons to be reduced to NO_2^- ions, inducing the increase of OH^- concentration (eq 3). More and more OH^- ions will combine with Zn^{2+} ions to form an intermediate growth unit of $Zn(OH)_4^{2-}$ (eq 4).[35] Due to heat convection, diffusion of ions, and deregulation movement among molecules and ions in solution, ZnO clusters are formed by the dehydration reaction between OH^- and H^+ ions (eq 5). It is well-known that supersaturation is a prerequisite for crystal growth in solution and is also intimately connected with growth processes involved in the evolution of crystal morphology.[36] As the reactions continue (eqs 4 and 5), more and more ZnO clusters appear in the solution, as proposed in step I of Figure 4. When the solution is supersaturated, nucleation begins, and then, ZnO nanocrystallites form in the solution, as shown in step II of Figure 4.

The following growth (step III of Figure 4) of the ZnO nanocrystallites can be considered as the incorporation of the intermediate growth unit $[Zn(OH)_4^{2-}]$ into the crystal lattices of the as-formed nanocrystallites by the dehydration reaction (eq 5). Therefore, the growth habit of as-grown ZnO nanocrystallites is determined by not only the internal structure of ZnO itself (thermodynamic factor) but also the concentration of OH^-, which is the main kinetic factor in this CBD growth process. Structurally, ZnO has three types of basal planes, a polar (0001) plane and two nonpolar $(2\bar{1}\bar{1}0)$ and $(01\bar{1}0)$ planes with C_{6v} symmetry. The low-symmetry, nonpolar $(2\bar{1}\bar{1}0)$ face is most stable with threefold-coordinated atoms. The large (0001) polar surface is generally energetically unfavorable unless the surface charges are compensated by passivating agents. Under thermodynamic equilibrium conditions, the fastest growth rate of ZnO is along the *c* axis due to the higher surface energy.[37] When the concentration of $Zn(NO_3)_2$ is low, the corresponding concentration of OH^- produced by eq 3 is also low, which has a smaller effect on the intrinsic growth habit of ZnO. In this case, the crystal growth rate along the <0001> direction is faster

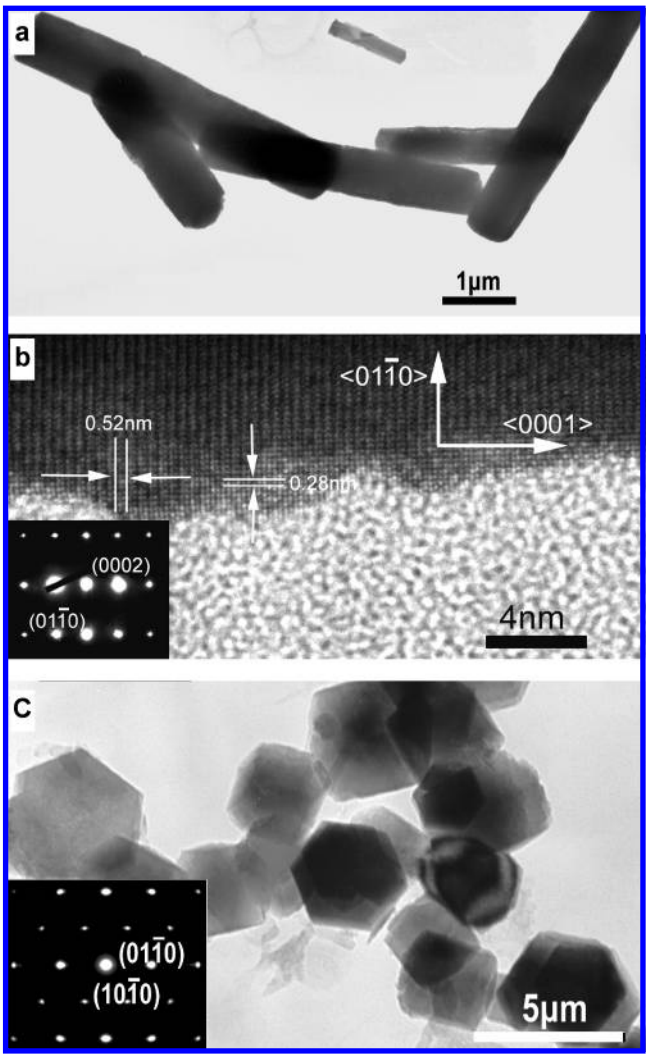

Figure 3. (a) TEM image of ZnO nanorods, (b) high-resolution TEM image of a ZnO nanorod and its corresponding SAED pattern (inset) and (c) TEM image and SAED pattern of ZnO nanoplates.

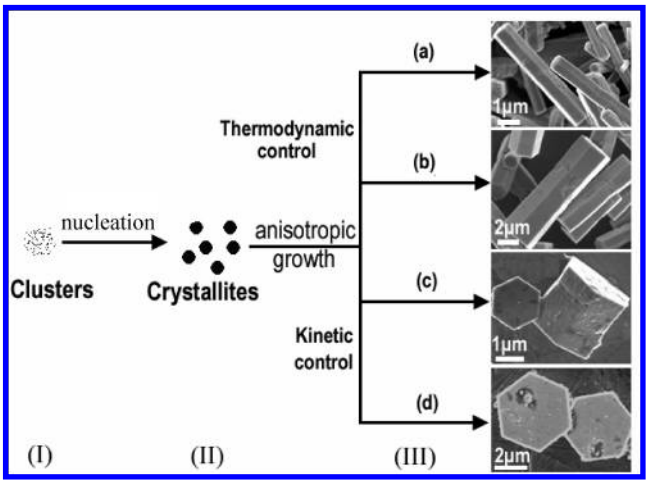

Figure 4. Illustration of the proposed growth mechanism of the ZnO nanostructures evolving from nanorods to nanoplates.

than that along <2$\bar{1}\bar{1}$0>. Therefore, the ZnO sample shows the morphology of a one-dimensional nanorod (Figure 4a), which is the typical result of its intrinsic growth habit. This is the most common case of ZnO nanostructure growth, which has been widely reported in other solution-[38] and vapor-phase methods.[2] When the concentration of $Zn(NO_3)_2$ is increased, the concentration of OH^- in solution will increase by two times (eq 2). It has been reported that the (0001) surfaces of ZnO with tetrahedral zincs usually have terminal OH^- ligands in solution.[39,40] These ligands will prevent the new $Zn(OH)_4^{2-}$ ions from incorporating effectively into the as-formed ZnO nanocrystallites along the *c*-axis direction. This means that the crystal growth along the <0001> direction is partially suppressed under this condition, whereas the nanocrystallites can still grow sideways along the <2$\bar{1}\bar{1}$0> directions. Therefore, when the concentration of $Zn(NO_3)_2$ is increased to 0.05 M, the ZnO nanorods become shorter and thicker, as shown in Figure 4b. Further increase of the $Zn(NO_3)_2$ concentration causes the formation of a mixture of ZnO nanorods and nanoplates (Figure 4c). It is noted that the ZnO nanorods in the mixture are much shorter and thicker than those in Figure 4a and b. Finally, when the concentration of $Zn(NO_3)_2$ is increased to 0.1 M, much purer ZnO nanoplates are formed (Figure 4d) as the crystal growth along the <001> direction is more effectively suppressed. On average, the aspect ratio of the ZnO samples is decreased with the increase of $Zn(NO_3)_2$ concentration. As a result, the ZnO morphology evolves from a one-dimensional nanorod to a two-dimensional nanoplate. This observation also goes well with the reports on other organic ligand-controlled crystallizations of ZnO crystals in the presence of diblock copolymers[7] or citrate salts.[8]

3.3. Cathodoluminescence Properties. The room-temperature CL spectra of the ZnO nanorods and nanosheets shown in Figure 5a exhibit the typical NBG UV emission band centered at 3.23 eV and a broad visible emission band, which is usually attributed to deep-level emission (DLE) caused by defects of oxygen vacancies.[23] The relative intensity ratio (UV/DLE) of nanorods is a little bigger than that of nanoplates, which means, in general, that the ZnO nanorods have a better crystal quality than the nanoplates. To exploit the origin of the NBG UV emission, low-temperature CL at 11 K of the ZnO nanorods and nanoplates was measured, as shown in Figure 5b. The spectra possess essentially similar optical properties. At low temperature, the NBG emissions are composed of three typical peaks. The most dominant emissions at 3.361 eV that are labeled as BEC (bound exciton complex) are in the spectral range of donor-bound excitons.[25] However, the line widths of the BECs are rather broad. This probably indicates that different kinds of donor species are involved and that their chemical natures are not clear. On the high-energy side of the BEC emission, no free exciton emissions are detected. However, on the low-energy side, a peak centered at 3.316 eV (labeled as SX) together with its LO phonon replica (SX-LO) at 3.244 eV is observed. To further study the optical characters of the ZnO nanostructures prepared by the solution method, temperature-dependent CL spectra were measured from 11 to 300 K, as shown in Figure 5c. By tracking the evolutions of different emission peaks from low temperatures, the composition of the NBG UV emission at room temperature can be disclosed. In this process, no free exciton emission was detected due to exciton delocalization in the nanostructures with increasing temperature, unlike the behavior in bulk ZnO material.[41] The BEC emission shows a continuous red shift due to the temperature-induced band gap shrinkage of ZnO, which can be well fitted by the Bose−Einstein model[42]

$$E_{BEC}(T) = E_{BEC}(0) - 2\alpha_B\Theta_B\left[\coth\left(\frac{\Theta_B}{2T}\right) - 1\right] \qquad (6)$$

with $E_{BEC}(0) = 3.362$ eV, $\alpha_B = 1.2 \times 10^{-4}$ eV/K, and $\Theta_B = 247$ K, as shown in Figure 5d. The fitted Bose−Einstein

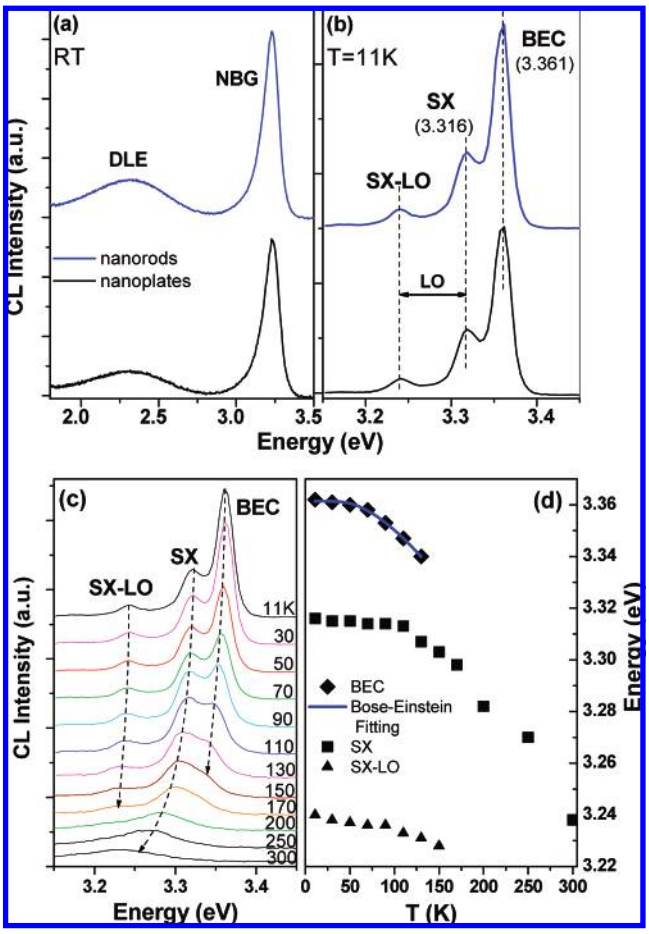

Figure 5. (a) Room-temperature CL and (b) low-temperature (11 K) CL spectra of the ZnO nanorods and nanoplates at the primary excitation voltage of 10 kV; (c) temperature-dependent CL spectra from 11 to 300 K; (d) CL peak energies versus temperatures taken from (c). Solid symbols (◆, ■, and ▲) are the experimental data, and the solid lines are fitted with the Bose−Einstein equation. Parameters are given in the text.

temperature is consistent with the data (240 K) in ref 24. Its intensity decreases gradually and eventually vanishes (>130 K) due to the ionization of the excitons from the donors. The SX emission also shows a continuous red shift with increasing temperature and becomes dominant when the temperature is above 110 K, as indicated by dashed line in Figure 5d. Above 150 K, the whole spectrum becomes featureless. Therefore, the main compositions of the room-temperature NBG UV emission are SX and its LO phonon replica, which is also different than the case of ZnO nanostructures prepared by vapor-phase methods.[43]

As for the assignment of the emission at ~3.31 eV, it is still a matter of controversy. Look et al.[44] and Xiu et al.[45] have assigned it to nitrogen- and phosphorus-related acceptor-bound exciton emission (A^0, X), respectively, for N- or P-doped ZnO films. However, there is no intensive dopant applied in the CBD method. Therefore, the assignment of the SX as intensively dopant-induced (A^0, X) emission can be ruled out in this case. As SX emission has a large binding (localization) energy (FX−SX, ~61 meV), which is similar to the excitonic binding energy of ZnO, it is expected that SX still has the nature of an exciton as long as the excitons govern the luminescence. As large concentrations of residual precursor ions are present in the reaction solution, it has been reported that they can adhere to the surface of these nanostructures as impurities.[46] Since these nanostructures have a large surface-to-volume ratio, these surface impurities have serious effects on the defect formation of ZnO crystals, especially the defect states on surfaces.[47] Therefore, it is expected that such surface states may play an important role in their excitonic optical properties. According to the above analysis, we propose that the recombination of excitons bound at these surface states causes the SX emission. This assignment is also consistent with the observation of the surface-related emissions of ZnO nanocrystals.[32] According to the theory prediction, these surface states are acceptor-like defects,[18] which may shed some light on the p-type doping of ZnO nanostructures.

4. Conclusions

In conclusion, we reported a controllable and low-temperature CBD solution method to prepare ZnO nanostructures with different morphologies. By changing the precursor concentration, the ZnO nucleation and growth process were regulated from a thermodynamically controlled process to a kinetically controlled process, with the result that the ZnO morphologies evolved from nanorods to nanoplates. Due to the high surface energy of the polar (0001) plane, the ZnO nanorods grow fast along the *c*-axis direction, which is the typical intrinsic growth habit of ZnO under thermodynamic equilibrium conditions. When the OH^- concentration is increased in precursor solution, more OH^- ions preferably adsorb on the (0001) planes of ZnO, which prevents the newly produced ZnO clusters from incorporating into the ZnO crystallites effectively. Therefore, the crystal growth of the ZnO crystallites along the *c* axis is partially suppressed. However, they can still grow sideways along the $<2\bar{1}\bar{1}0>$ directions, leading to the decrease of the aspect ratio of the ZnO nanorod. Finally, two-dimensional ZnO nanoplates are formed. Low-temperature CL spectra of such ZnO nanostructures exhibit donor-bound exciton emission and a typical SX emission at ~3.31 eV. We propose the surface-state-related exciton emission as its possible assignment. With increasing temperature, the donor-bound exciton emission decreases gradually due to the ionization of donors and finally vanishes when temperature is above 130 K. The near-band-gap ultraviolet emission at room temperature is dominated by the surface-related exciton emission. It is suggested that the use of such nanorods or nanoplates prepared via the solution method at room temperature as optoelectronic devices needs to control or passivate their surface-related states.

Acknowledgment. This work was financially supported by the major state research program of China "Fundamental Investigation on Micro-Nano Sensors and Systems based on BNI Fusion" (Grant No. 2006CB300402), the Natural Science Foundation of China (Grant No. 50671100), and the fund for Excellent CAS Presidential Award of Chinese Academy of Sciences (B.C.). The authors also thank Professor Grundmann at Universitaet Leipzig for the use of their CL facilities.

References and Notes

(1) Norton, D. P.; Heo, Y. W.; Ivill, M. P.; Ip, K.; Pearton, S. J.; Chisholm, M. F.; Steiner, T. *Mater. Today* **2004**, *7*, 34.
(2) Wang, Z. L. *J. Phys.: Condens. Matter* **2004**, *16*, R829.
(3) Heo, Y. W.; Norton, D. P.; Tien, L. C.; Kwon, Y.; Kang, B. S.; Ren, F.; Pearton, S. J.; LaRoche, J. R. *Mater. Sci. Eng. R* **2004**, *47*, 1.
(4) Zhang, W. X.; Yanagisawa, *Chem. Mater*. **2007**, *19*, 2329.
(5) Hu, J. Q.; Bando, Y.; Zhan, J. H.; Li, Y. B.; Sekiguchi, T. *Appl. Phys. Lett.* **2003**, *83*, 4414.
(6) Fan, H. J.; Scholz, R.; Kolb, F. M.; Zacharias, M.; Goesele, U.; Heyroth, F.; Eisenschmit, C.; Hempel, T.; Christen, J. *Appl. Phys. A* **2004**, *79*, 1895.
(7) Peng, Y.; Xu, A. W.; Deng, B.; Antonietti, M.; Coelfen, H. *J. Phys. Chem. B* **2006**, *110*, 2988.

(8) Tian, Z. R.; Voigt, J. A.; Liu, J.; Mckenzie, B.; Mecdermott, M. J.; Rodriguez, M. A.; Konishi, H.; Xu, H. F. *Nat. Mater.* **2003**, *2*, 821.
(9) Xu, C. X.; Sun, X. W.; Dong, Z. L.; Yu, M. B. *Appl. Phys. Lett.* **2004**, *85*, 3878.
(10) Li, F.; Ding, Y.; Gao, P. X.; Xin, X. Q.; Wang, Z. L. *Angew. Chem., Int. Ed.* **2004**, *43*, 5238.
(11) Illy, B.; Shollock, B. A.; MacManus-Driscoll, J. L.; Ryan, M. P. *Nanotechnology* **2005**, *16*, 320.
(12) Cao, B. Q.; Cai, W. P.; Li, Y.; Sun, F. Q.; Zhang, L. D. *Nanotechnology* **2005**, *16*, 1734.
(13) Hosono, E.; Fujihara, S.; Honoma, I.; Zhou, H. S. *Adv. Mater.* **2005**, *17*, 2091.
(14) Wang, Z. L. *MRS Bull.* **2007**, *32*, 109.
(15) Niesen, T. P.; De Guire, M. R. *J. Electroceram.* **2001**, *6*, 169.
(16) Izaki, M. *Chem. Commun.* **2002**, 476.
(17) Govender, K.; Boyle, D. S.; Kenway, P. B.; O'Brien, P. *J. Mater. Chem.* **2004**, *14*, 2575.
(18) Fonoberov, V. A.; Balandin, A. A. *Appl. Phys. Lett.* **2004**, *85*, 5971.
(19) Fonoberov, V. A.; Alim, K. A.; Balandin, A. A.; Xiu, F. X.; Liu, J. L. *Phys. Rev. B* **2006**, *73*, 165317.
(20) Zhang, B. P.; Binh, N. T.; Segawa, Y.; Kashiwaba, Y.; Haga, K. *Appl. Phys. Lett.* **2004**, *84*, 586.
(21) Cao, B. Q.; Cai, W. P.; Zeng, H. B. *Appl. Phys. Lett.* **2006**, *88*, 161101.
(22) Cho, Y. H.; Kim, J. Y.; Kwack, H. S.; Kwon, B. J.; Dang, L. S.; Ko, H. J.; Yao, T. *Appl. Phys. Lett.* **2006**, *89*, 201903.
(23) Cao, B. Q.; Cai, W. P.; Zeng, H. B.; Duan, G. T. *J. Appl. Phys.* **2006**, *99*, 073516.
(24) Wang, L. J.; Giles, N. C. *J. Appl. Phys.* **2003**, *94*, 973.
(25) Meyer, B. K.; Alves, H.; Hofmann, D. M.; Kriegseis, W.; Forster, D.; Bertram, F.; Christen, J.; Hofmann, A.; Strassburg, M.; Dworzak, M.; Haboeck, U.; Rodina, A. V. *Phys. Status Solidi B* **2004**, *241* 231.
(26) Zhang, X. Q.; Yao, Z. G.; Huang, S. H.; Suemune, I.; Kumano, H. *J. Appl. Phys.* **2006**, *99*, 063709.
(27) Hamby, D. W.; Lucca, D. A.; Klopfstein, M. J.; Cantwell, G. *J. Appl. Phys.* **2003**, *93*, 3214.
(28) Shan, W.; Walukiewicz, W.; Ager, J. W., III; Yu, K. M.; Yuan, H. B.; Xin, H. P.; Cantwell, G.; Song, J. J. *Appl. Phys. Lett.* **2005**, *86*, 191911.
(29) Najafov, H.; Fukada, Y.; Ohshio, S.; Iida, S.; Siatoh, H. *Jpn. J. Appl. Phys., Part 1* **2003**, *42*, 3490.
(30) Bekeny, C.; Voss, T.; Gafsi, H.; Gutowski, J.; Postels, B.; Kreye, M.; Waag, A. *J. Appl. Phys.* **2006**, *100*, 104317.
(31) Gorl, C. R.; Emanetoglu, N. W.; Liang, S.; Mayo, W. E.; Lu, Y.; Wraback, M.; Shen, H. *J. Appl. Phys.* **1999**, *85*, 2595.
(32) Fallert, J.; Hauschild, R.; Stelzl, F.; Urban, A.; Wissinger, M.; Zhou, H. J.; Klingshirn, C.; Kalt, H. *J. Appl. Phys.* **2007**, *101*, 073506.
(33) Lorenz, M.; Lenzner, J.; Kaidashev, E. M.; Hochmuth, H.; Grundmann, M. *Ann. Phys.* **2004**, *13*, 39.
(34) Izaki, M.; Shinoura, O. *Adv. Mater.* **2001**, *13*, 142.
(35) Li, W. J.; Shi, E. W.; Zhong, W. Zh.; Yin, Zh. W. *J. Cryst. Growth* **1999**, *203*, 186.
(36) Mullin, J. W. *Crystallization*; Butterworth-Heinemann: Woburn, MA, 1997.
(37) Kong, X. Y.; Wang, Z. L. *Appl. Phys. Lett.* **2004**, *84*, 975.
(38) Vayssieres, L. *Adv. Mater.* **2003**, *15*, 464.
(39) Slunecko, J.; Kosec, M. *J. Am. Ceram. Soc.* **1998**, *81*, 1121.
(40) Dutta, P. K.; Gallagher, P. K.; Twa, J. *Chem. Mater.* **1992**, *4*, 847.
(41) Grabowska, J.; Meaney, A.; Nanda, K. K.; Mosnier, J. P.; Henry, M. O.; Duclćre, J. R.; McGlynn, E. *Phys. Rev. B* **2005**, *71*, 115439.
(42) O'Donnell, K. P.; Chen, X. *Appl. Phys. Lett.* **1991**, *58*, 2924.
(43) Wischmeier, L.; Bekeny, C.; Voss, T.; Boerner, S.; Schade, W. *Phys. Status Solidi B* **2006**, *243*, 919.
(44) Look, D. C.; Reynolds, D. C.; Litton, C. W.; Jones, R. L.; Eason, D. B.; Cantwell, G. *Appl. Phys. Lett.* **2002**, *81*, 1830.
(45) Xiu, F. X.; Yang, Z.; Mandalapu, L. J.; Liu, J. L. *Appl. Phys. Lett.* **2006**, *88*, 152116.
(46) Hirano, S.; Takeuchi, N.; Shimada, S.; Masuya, K.; Ibe, K.; Tsunakawa, H.; Kuwabara, M. *J. Appl. Phys.* **2005**, *98*, 094305.
(47) Shalish, I.; Temkin, H.; Narayanamurti, V. *Phys. Rev. B* **2004**, *69*, 245401.